



NRC Publications Archive Archives des publications du CNRC

Effect of the oxygen content in solution on the static and cyclic deformation of titanium foams

Lefebvre, L.-P.; Baril, É.; Bureau, M. N.

This publication could be one of several versions: author's original, accepted manuscript or the publisher's version. / La version de cette publication peut être l'une des suivantes : la version prépublication de l'auteur, la version acceptée du manuscrit ou la version de l'éditeur.

For the publisher's version, please access the DOI link below. / Pour consulter la version de l'éditeur, utilisez le lien DOI ci-dessous.

Publisher's version / Version de l'éditeur:

<https://doi.org/10.1007/s10856-009-3798-x>

Journal of Materials Science: Materials in Medicine, 20, 11, pp. 2223-2233, 2009

NRC Publications Record / Notice d'Archives des publications de CNRC:

<https://nrc-publications.canada.ca/eng/view/object/?id=05a18aa7-60bd-463a-9076-b2ad964ec385>

<https://publications-cnrc.canada.ca/fra/voir/objet/?id=05a18aa7-60bd-463a-9076-b2ad964ec385>

Access and use of this website and the material on it are subject to the Terms and Conditions set forth at

<https://nrc-publications.canada.ca/eng/copyright>

READ THESE TERMS AND CONDITIONS CAREFULLY BEFORE USING THIS WEBSITE.

L'accès à ce site Web et l'utilisation de son contenu sont assujettis aux conditions présentées dans le site

<https://publications-cnrc.canada.ca/fra/droits>

LISEZ CES CONDITIONS ATTENTIVEMENT AVANT D'UTILISER CE SITE WEB.

Questions? Contact the NRC Publications Archive team at

PublicationsArchive-ArchivesPublications@nrc-cnrc.gc.ca. If you wish to email the authors directly, please see the first page of the publication for their contact information.

Vous avez des questions? Nous pouvons vous aider. Pour communiquer directement avec un auteur, consultez la première page de la revue dans laquelle son article a été publié afin de trouver ses coordonnées. Si vous n'arrivez pas à les repérer, communiquez avec nous à PublicationsArchive-ArchivesPublications@nrc-cnrc.gc.ca.



1

2 Effect of the oxygen content in solution on the static and cyclic 3 deformation of titanium foams

4 L. P. Lefebvre · E. Baril · M. N. Bureau

5 Received: 9 January 2009 / Accepted: 2 June 2009
6 © Her Majesty the Queen in Right of Canada 2009

7 **Abstract** It is well known that interstitials affect the
8 mechanical properties of titanium and titanium alloys.
9 Their effects on the fatigue properties of titanium foams
10 have not, however, been documented in the literature. This
11 paper presents the effect of the oxygen content on the static
12 and dynamic compression properties of titanium foams.
13 Increasing the oxygen content from 0.24 to 0.51 wt% O in
14 solution significantly increases the yield strength and
15 reduces the ductility of the foams. However, the fatigue
16 limit is not significantly affected by the oxygen content and
17 falls within the 92 MPa ± 12 MPa range for all specimens
18 investigated in this study. During cyclic loading, deforma-
19 tion is initially coming from cumulative creep followed
20 by the formation of microcracks. The coalescence of these
21 microcracks is responsible for the rupture of the specimens.
22 Fracture surfaces of the specimens having lower oxygen
23 content show a more ductile aspect than the specimens
24 having higher oxygen content.

27 1 Introduction

28 Porous titanium coatings have been used for many years in
29 different load bearing orthopedic applications. These sur-
30 faces were initially proposed in the late 60's as a solution to
31 problems encountered with methacrylate-based bone cement
32 used for orthopedic implant fixation [1, 2]. These coatings
33 have high roughness, increase the friction between the
34 implant and surrounding bone and provide the initial stability

A1 L. P. Lefebvre (✉) · E. Baril · M. N. Bureau
A2 National Research Council Canada/Industrial Materials Institute,
A3 75 de Mortagne, Boucherville, QC J4B 6Y4, Canada
A4 e-mail: louis-philippe.lefebvre@cnrc-nrc.gc.ca

to the implants. Besides, the interconnected porosity allows
bone tissue ingrowth that secures the long-term fixation and
stability of the implant. This approach is now widely used in
various hip and knee cementless procedures and most
orthopedic implant manufacturers are now commercializing
implants with these coatings.

Research has recently switched from thin porous bead
coatings, sintered mesh and thermal sprayed rough coatings
to metallic foams. These foams have been used in the
development of various new and improved treatments such
as bone augmentation and graft free vertebra fusion for the
treatment of degenerative disk diseases. These foams have
the advantage of being much more porous than the tradi-
tional sintered beads or mesh and plasma spray coating.
The increased porosity provides elastic modulus much
closer to those of bones, more space for bone in-growth and
interlocking as well as more surface for bone-implant
contact.

It is well established that the mechanical properties of
dense titanium and titanium alloys are sensitive to the
presence of interstitial solutes such as oxygen, nitrogen,
carbon and hydrogen. These interstitials increase the elastic
modulus, the yield strength and reduces the ductility of
titanium and titanium alloys [3]. Nitrogen has generally the
most significant effect, followed by oxygen and carbon.
While nitrogen and carbon are usually not found at high
concentration in dense titanium, oxygen is a common
contaminant due to the high affinity of titanium for oxygen
and its high solubility in titanium. At low concentration,
oxygen occupies octahedral sites of the α -titanium crystal
and increases the lattice parameters as well as the c/a
ratio in the crystal, resulting in a volumetric change of
0.0013 nm³ per atomic percent of oxygen [4, 5]. The
oxygen atoms interact with the hydrostatic stress field of
the dislocations but also with the shear stress field, so that

35
36
37
38
39
40
41
42
43
44
45
46
47
48
49
50
51
52
53
54
55
56
57
58
59
60
61
62
63
64
65
66
67
68
69

AUTHOR PROOF

70 both edge and screw dislocation motions are affected.
71 Therefore, increasing oxygen content results in an increase
72 of the yield strength, hardness and fatigue resistance at a
73 given stress level, whereas it decreases the ductility and
74 impact resistance by restricting twinning and prismatic slip
75 [6].

76 Since interstitials significantly affect the properties of
77 titanium, standards have been established on the chemical
78 requirements for the use of dense titanium in orthopedic
79 and dental applications [7–11]. A standard has also been
80 developed for porous titanium coating for the production of
81 surgical implants [12]. According to this standard, the
82 maximum content of oxygen in the powder used for such
83 coatings must be lower than 0.4 wt% O. The standard does
84 not, however, specify the amount of oxygen in solution in
85 the final coating.

86 The effect of porous coating on the fatigue properties of
87 Ti-6Al-4V implants have been reported in the literature
88 [13–15]. It is recognized that porous coating reduces the
89 fatigue strength of the implants. This reduction is associ-
90 ated with the modification of the microstructure during the
91 high temperature sintering treatment as well as with the
92 stress concentration coming from the surface irregularities
93 at the sintered bond sites on the surface of the implants.
94 The fatigue properties of tantalum and nickel-titanium
95 foams intended for biomedical applications have also been
96 reported in the literature. The compressive fatigue limits
97 reported by [16–18] are 7.5 MPa at 10^8 cycles for 63–68%
98 open porosity nickel-titanium foams and 13.2 MPa at
99 10^8 cycles for 65–70% open porosity tantalum foams. In
100 another study by [19], the compressive fatigue limit of
101 75–85% porous tantalum foams is around 23 MPa at
102 5×10^6 . Variations in the results presented in the later
103 study were significant and reported to be dependant upon
104 the nature of the material tested.

105 No studies are available on the fatigue properties of pure
106 titanium foams as well as on the effect of the oxygen
107 content on the fatigue of these materials. This probably
108 comes from the fact that these materials are relatively new.
109 The limited information available can also be attributed to
110 challenges associated with the production of materials with
111 the exact same structure but with different level of oxygen
112 in solution. Difficulties also come from the discrimination
113 of the amount of oxygen in solution from the oxygen in the
114 oxide layer on the surface of the foam. Due to the high
115 specific surface area of the materials, the relative contri-
116 bution of the amount of oxygen coming from the oxide
117 formed on the surface of the foam must be taken into
118 account when determining the effect of oxygen on the
119 properties of these materials.

120 This paper describes the compression static and dynamic
121 properties of titanium foams having different oxygen
122 contents. The titanium foam was produced with a powder

metallurgy process. The foam samples were oxidized at 123
low temperature to obtain different oxygen concentrations. 124
They were then treated at 1000°C to dissolve the surface 125
oxide and obtain solid solutions with different oxygen 126
levels. The resulting titanium foam samples showed the 127
same structure but different oxygen contents. They were 128
then tested in compression under static (monotonic and 129
creep at room temperature) and cyclic loading to investi- 130
gate the effect of oxygen on their properties. The fatigue 131
behavior of the titanium foams was done under compres- 132
sion-compression fatigue, i.e. with a non-zero mean stress. 133

2 Experimental procedure 134

135 Titanium foams were produced using a process described
136 elsewhere [20]. Briefly, spherical pure titanium powder
137 (AP&C Advanced Powders and Coatings Inc., Quebec,
138 Canada; $-180 \mu\text{m}$) was admixed with a polyethylene binder
139 and a chemical foaming agent (p,p'-oxybis[benzenesulfonyl
140 hydrazide]). The resulting powder mixture was poured into a
141 cylindrical mold and heated up in air at 210°C to foam the
142 material. The resulting material was then successively
143 debinded at 450°C in Ar (10^{-8} ppm O_2) and sintered
144 at 1400°C under vacuum (10^{-5} – 10^{-6} Torr range). To
145 increase their oxygen content, the resulting foam cylinders
146 were treated in Ar-20% O_2 at 3 different temperatures
147 (300–450°C). Using this method, foams with 3 different
148 oxygen concentrations were produced. Material A refers to
149 the foam with the lowest oxygen content in solution
150 (0.24 wt%), Material B is the foam with the intermediate
151 oxygen content (0.42 wt% in solution) while material C
152 refers to the foam with the highest oxygen concentration
153 (0.51 wt% O in solution). The oxidized cylinders were
154 solution treated for 1 h at 1000°C to dissolve the oxide layer
155 and bring the oxygen into solid solution in titanium. After
156 cooling, a thin oxide layer was reformed on the Ti surface
157 (typically 5 nm, as described in [21]). Table 1 summarized
158 the properties of the foams characterized in this study.

159 The density of the specimens was evaluated using the
160 weight (Ohaus, Explorer, 210 g \pm 0.1 mg) and physical

Table 1 Characteristics of the titanium foams characterized in this study

	A	B	C
Density (% theoretical)	51	51	51
Surface area (m^2/g)	0.05	0.05	0.05
Total oxygen content (wt%)	0.3	0.48	0.57
Oxide thickness (nm)	5	5	5
Oxygen in solution (wt%)	0.24	0.42	0.51
Yield strength (MPa)	129	162	178

161 dimensions of the cylinders. Specimens were observed
 162 with an optical microscope, a JEOL 6100 scanning electron
 163 microscope (SEM), an Hitachi S-4700 field-emission gun
 164 scanning electron microscope (FEG-SEM) and a X-Tek
 165 HMXST 225 X-ray microtomograph (μ CT). The specific
 166 surface area was evaluated by gas adsorption (BET) using a
 167 Micrometrics ASAP 2010 system with krypton as adsorbate.
 168 Oxygen content was evaluated using an inert gas
 169 fusion technique with a LECO TCH-600 analyzer. The
 170 amount of oxygen in the oxide film was estimated using a
 171 method described in [21] based on the evaluation of the
 172 weight gain associated with the formation of the oxide film
 173 after the sintering treatment. The amount of oxygen in
 174 solution was deducted from the total measured amount of
 175 oxygen (LECO) and the estimated amount of oxygen in the
 176 oxide film. Compression testing was done on a MTS
 177 100 kN testing machine. Cyclic tests were done under
 178 sinusoidal 10 Hz cycling (deformation rate of approxi-
 179 mately 1 mm/s) and a load ratio ($R = \sigma_{\min}/\sigma_{\max}$) of 0.1.
 180 The tests were ended either at a user defined deformation of
 181 22.5% or at 5×10^6 cycles (defined as no rupture). The
 182 cyclic tests were done on 11 specimens for materials A and
 183 B and 6 specimens for material C. Monotonic tests were
 184 performed at a crosshead speed of 1.25 mm/min to deter-
 185 mine the effect of oxygen on the yield strength. Some tests
 186 were interrupted at 22.5% deformation to compare the
 187 level of damage (i.e. cracks) in the specimens deformed
 188 monotonically with those deformed under cyclic loading.
 189 Creep tests were also done under a static load (107 MPa) to
 190 determine the creep contribution to the total deformation
 191 under cyclic loading. All tests were done at room tem-
 192 perature in air. Cumulative deformation and deformation
 193 amplitude were measured using a platen-mounted LVDT
 194 transducer (Intertechnology, Don Mills, Canada, model
 195 0243-000).

196 3 Results

197 A general view of the cylinders before compression is
 198 presented in Fig. 1. The specimens are 51% dense and
 199 consisted in a continuous network of open porosity. The
 200 pore diameters are typically between 50 and 400 μ m, as
 201 determined visually on the SEM micrographs. Pycnometry
 202 measurements showed that the porosity is completely open.
 203 Besides, the material has a granular structure associated
 204 with the powder metallurgy process used. Polished cross
 205 sections (Fig. 2) and SEM micrographs (Fig. 3a) reveal
 206 that the particles are well sintered together. At high mag-
 207 nification, fine surface features can be observed (Fig. 3b,
 208 d). These features were produced by thermal etching during
 209 sintering as a result of the evaporation/condensation and
 210 surface diffusion of titanium occurring at high temperature

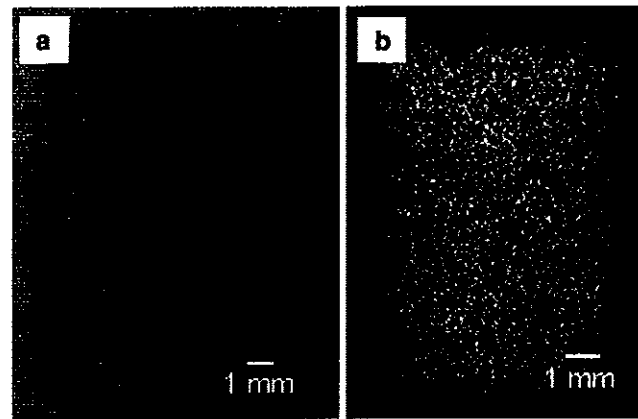


Fig. 1 Specimens characterized in the study a general view and b 2D cross section obtained from the reconstruction of microtomographic images

during sintering. These fine sub-micron features on the surface of the material account for its high specific surface area (0.05 m^2/g as evaluated by BET). Accordingly, due to the presence of the thin oxide film naturally formed on the surface of titanium (typically 5 nm in the present case), the thermal-etching lines contribute to the total oxygen content of the material.

The total amount of oxygen in the specimens produced is 0.3, 0.48 and 0.57 wt% (Table 1). When the oxygen contribution of the natural oxide formed on the surface of titanium is taken into account (i.e. 0.06 wt%), the calculated amount of oxygen in solution are 0.24, 0.42 and 0.51 wt%. The total carbon content is approximately 0.3 wt%. Carbon comes mainly from the foaming agent decomposition products. Carbon present in the foaming agent reacts with titanium and forms biocompatible carbides during debinding and sintering (Fig. 2b). Table 1 summarizes the densities, surface area and composition of the foam samples characterized in this study.

The monotonic compression behavior of the foam cylinders containing 0.24 and 0.51 wt% O in solution is presented in Fig. 4. The curves are characteristic of compression curve of ductile porous materials showing three stages: the initial elasto-plastic loading, the plastic deformation plateau and the consolidation stage at the end of the compression tests. The vertical lines visible on the curve come from unloading done during the compression tests to evaluate the elastic modulus (not presented in this study). The shape of the curves changes when the oxygen content in solution increases. Indeed, the yield strength (defined in this study as the intersection of the lines parallel to the stage 1 and 2 in the monotonic compression curves) increases significantly when the oxygen content in solution increases, as reported in Fig. 5. In addition, the densification stage occurs at larger deformation and the slope of the

Fig. 2 Optical micrographs of the polished cross section of a 0.24 wt% O specimen: **a** low magnification and **b** high magnification micrograph with arrows pointing at carbides

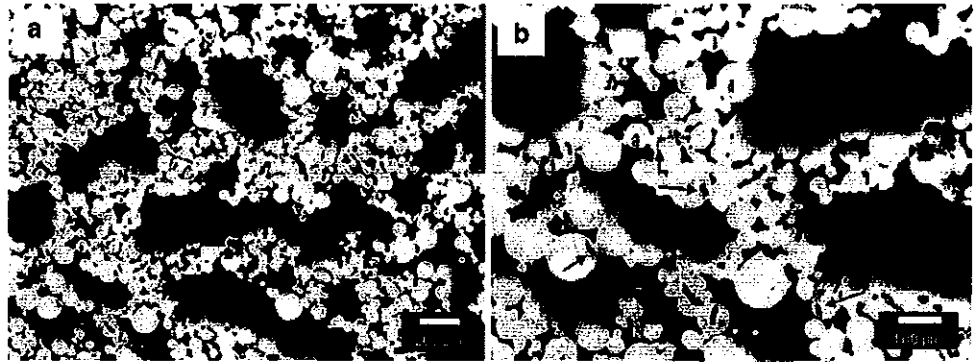
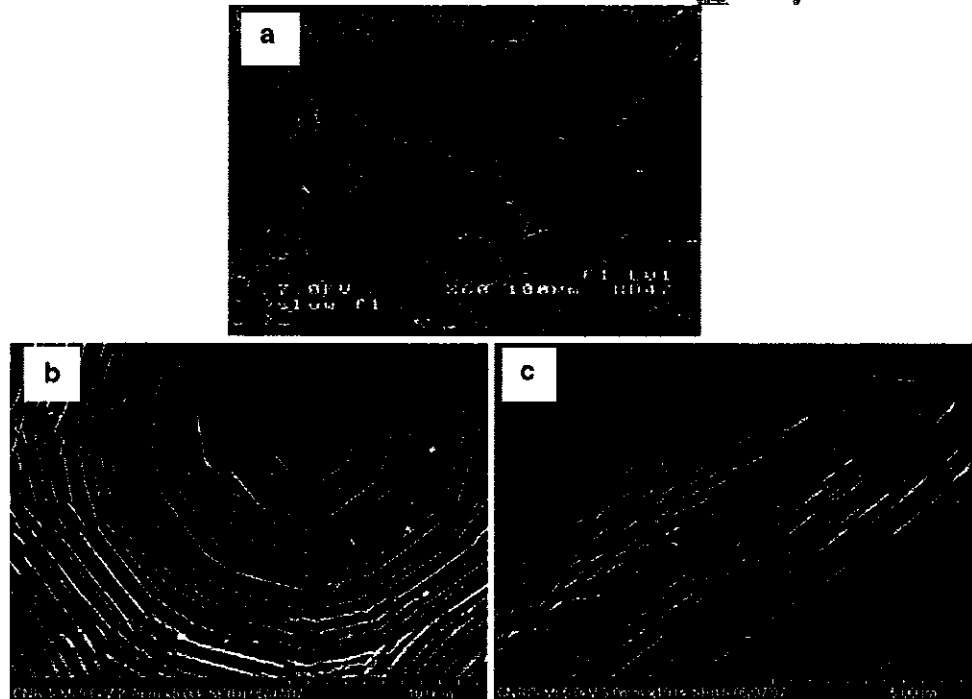


Fig. 3 SEM micrographs of a foam **a** low magnification, **b** high magnification presenting the etching lines on the surface of the particles and **c** high magnification showing a close-up at the submicronic thermal etching lines



246 densification is smaller when the amount of oxygen
247 increases (Fig. 4).

248 While all specimens exhibited smooth curves typical of
249 ductile foams, only the specimens containing small amount
250 of oxygen (i.e. 0.24 wt%) deformed plastically up to the
251 end of the tests. Indeed, when the amount of oxygen in
252 solution is large, the specimens showed severe cracks and
253 small pieces of material were ejected during the tests.
254 Figure 6 presents specimens containing two oxygen con-
255 tents (0.24% and 0.51 wt%) that were submitted to 22.5%
256 deformation under monotonic loading, which is equivalent
257 to the maximum deformation limit imposed during the
258 fatigue tests done in this study. On one hand, the specimens
259 with 0.24 wt% O did not show apparent cracks at their
260 surfaces (Fig. 6a). The observation of the internal structure
261 of these specimens using microtomography (Fig. 7a) and
262 optical microscopy on polished cross sections (Fig. 7b)
263 confirmed that only few microcracks were formed after

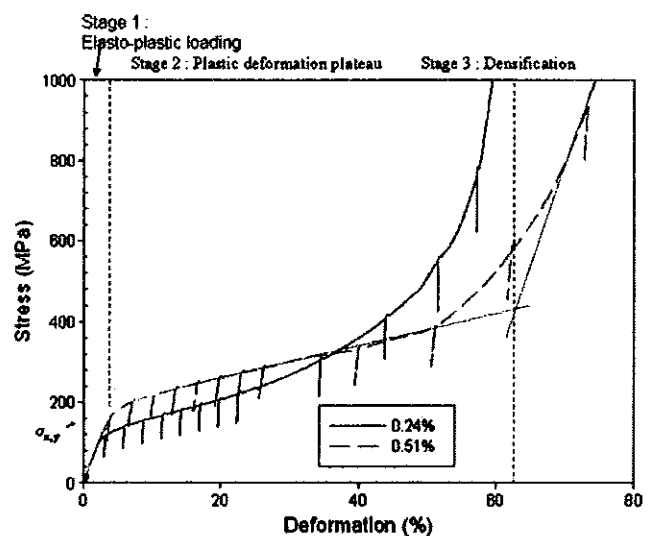


Fig. 4 Compression curves of titanium foams having two different oxygen contents in solution

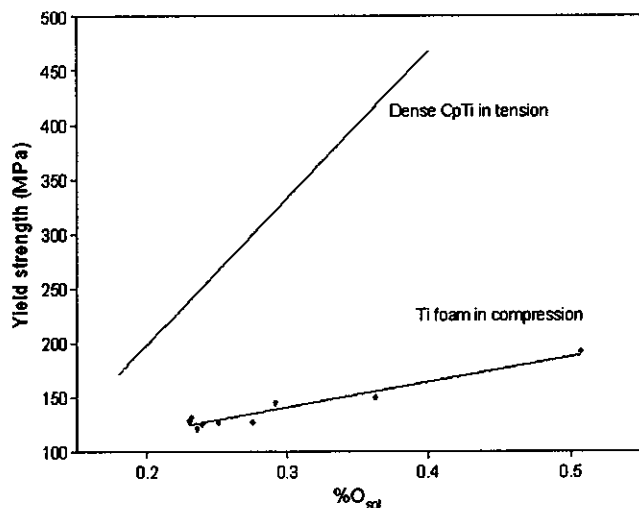
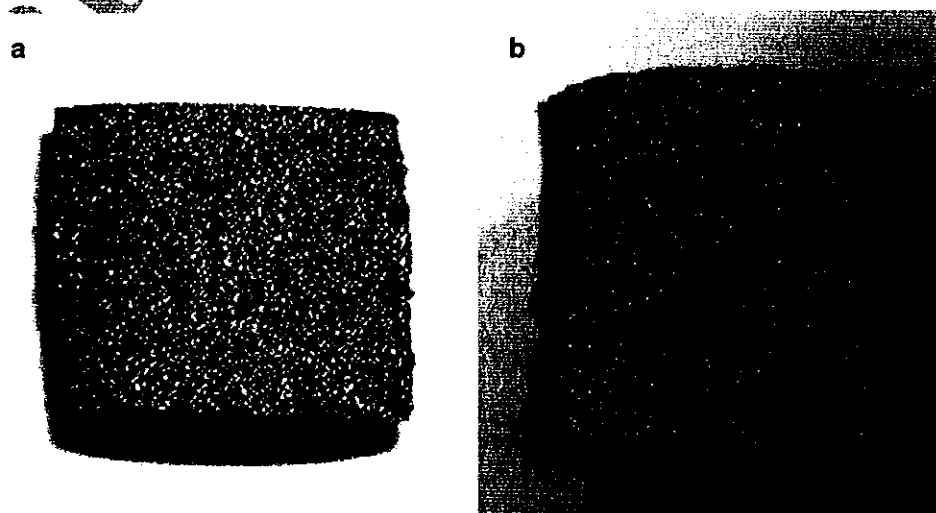


Fig. 5 Effect of oxygen content in solution on the yield strength of the Ti foams in compression and dense Ti in tension (from Refs. [7] and [21])

264 22.5% deformation in the 0.24 wt% O specimens. On the
 265 other hand, the specimens containing 0.51 wt% O in
 266 solution had significantly more cracks visible on their
 267 external surfaces (Fig. 6b) and in the internal structure after
 268 monotonic compression.

269 The cumulative cyclic deformation curves for specimens
 270 having two levels of oxygen in solution (0.24 and 0.51 wt%
 271 O) is presented in Fig. 8. At low stress level, the average
 272 deformation increases monotonically. The final cumulative
 273 deformation of the specimens is relatively low and similar
 274 for both oxygen contents. No crack or microcrack was
 275 observed on the external surfaces or polished cross sections.
 276 At higher stress levels, the cumulative deformation slowly
 277 raises up to a point where it strongly increases during the
 278 collapse stage.

Fig. 6 General view of specimens after 22.5% deformation under monotonic compression: a 0.24 wt% O and b 0.51 wt% O specimens



279 The deformation amplitude at the beginning of the tests
 280 (Fig. 9) is similar and is not affected by the oxygen content
 281 because the elastic modulus is similar for all materials
 282 and the applied stress is lower than the materials yield
 283 strength. Prior to their collapse, the deformation amplitude
 284 is approximately constant, in agreement with the cumulative
 285 deformation curves shown in Fig. 8. However, during
 286 the collapse stage, an increase of the deformation amplitude
 287 is observed, again in agreement with the cumulative
 288 deformation curves shown in Fig. 8. It should be noted that
 289 the sudden decrease in deformation amplitude observed in
 290 some of the longer fatigue tests (i.e. >10⁶ cycles), as
 291 observed in the 0.24 wt% O specimen tested at 83 MPa, is
 292 related to a sudden displacement of the LVDT transducer
 293 during the fatigue tests due to a lack of lubricant used to
 294 prevent the friction between the pin and the cylinder of the
 295 LVDT transducer.

296 The specimens that failed during the fatigue tests
 297 (defined at 22.5% of cumulative deformation) show cracks
 298 on their external surface for all oxygen levels (Fig. 10a, b).
 299 Slices from μ CT reconstruction showing the internal
 300 structure of specimens having 2 different oxygen contents
 301 (Fig. 10c, d) present the formation of crush bands and
 302 internal cracks (45° to the loading direction). Evidence of
 303 cell-collapse in the direction parallel to the applied stress
 304 can also be observed. The metallographic cross sections
 305 show several microcracks distributed throughout the spec-
 306 imens (see arrows in Fig. 11). The crack propagation does
 307 not seem, however, to be affected by the presence of the
 308 carbides. In fact, the cracks propagate at the necks between
 309 former powder particles but also within the particles. Very
 310 few cracks are located in the vicinity of the carbides.

311 The total cumulative deformation as a function of
 312 the loading time for foam specimens containing 0.24 wt% O
 313 in solution tested at 107 MPa under cyclic loading (fatigue,

Fig. 7 Cross section of the 0.24 wt% O specimens after 22.5% deformation under monotonic compression a 2D microtomography cross section presenting the general view of the specimen and b polished cross section presenting a closer view of the microstructure

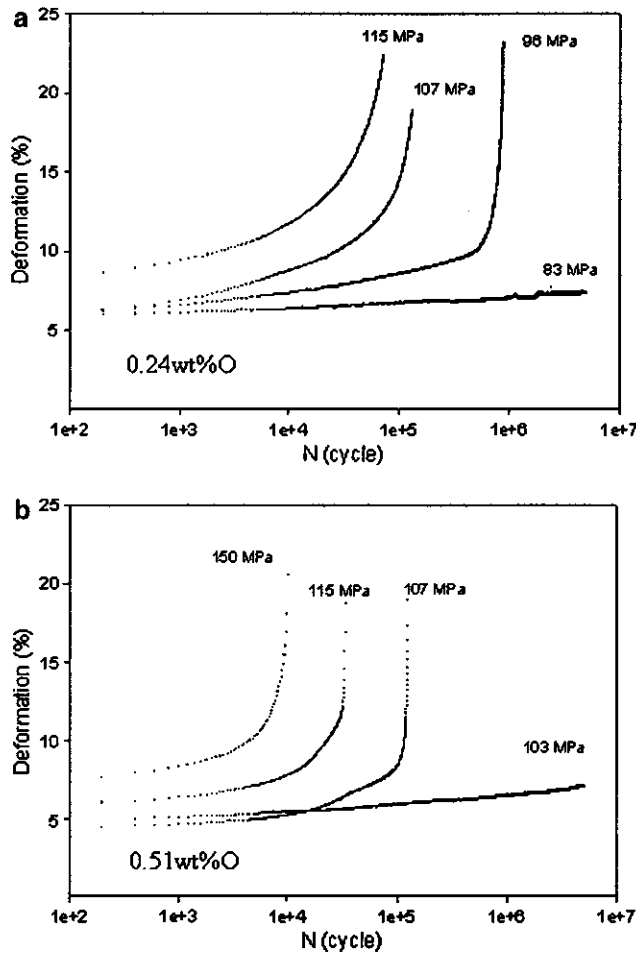
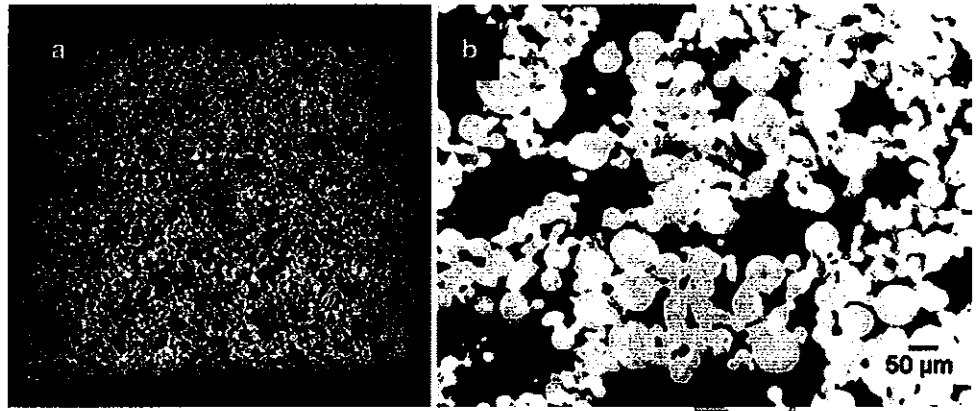


Fig. 8 Cumulative deformation versus cycle at different applied stresses for foams containing different amounts of oxygen in solution: a 0.24 and b 0.51 wt% O

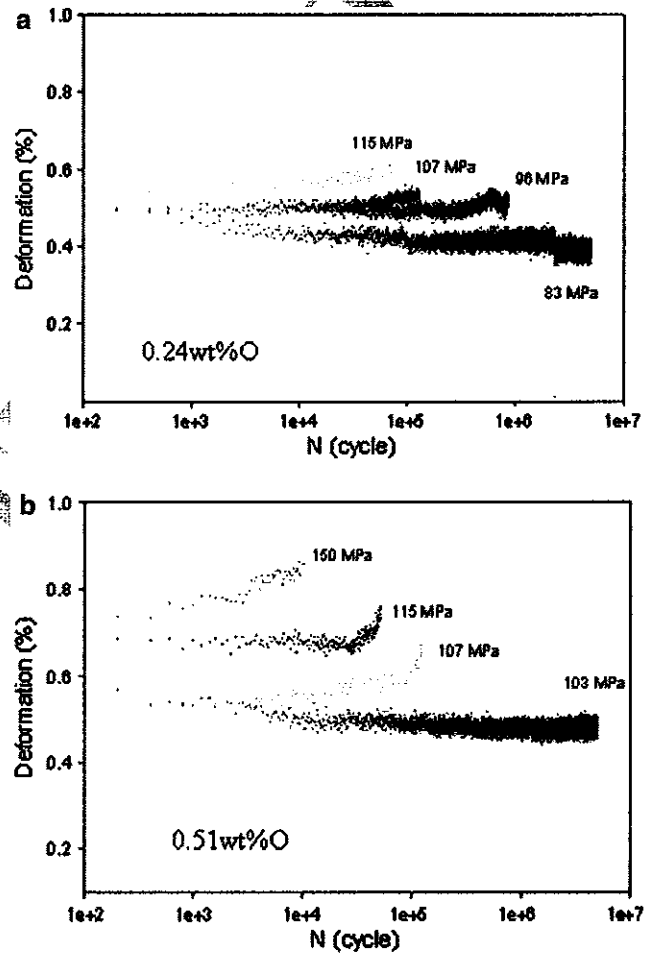


Fig. 9 Deformation amplitude versus cycle at different applied stresses for foams containing different amounts of oxygen in solution: a 0.24 and b 0.51 wt% O

314 10 Hz, $R = 0.1$) and tested at 107 MPa under static loading
 315 (creep) is presented in Fig. 12. The cyclic curve presents
 316 three stages (i.e., creep like, creep + initiation and propaga-
 317 tion, crack coalescence). Beside, the static curve has only
 318 one and is linear. The slope of the static curve is similar to the
 319 slope of the initial portion of the cyclic curve.

The S-N curves for materials with three levels of oxygen in solution (0.24, 0.42 and 0.51 wt% O) is presented in Fig. 13. The number of cycles to failure criteria is defined as the intersection of the lines adjacent to the first and third stage of the cumulative deformation vs. cycle curves. No clear difference between the three series of

Fig. 10 Specimens at the end of the fatigue tests at 107 MPa (22.5% total deformation): **a** general view of the 0.24 wt% O specimen, **b** general view of the 0.51 wt% O specimen, **c** internal structure of a 0.24 wt% O specimen observed by microtomography, **d** internal structure of 0.51 wt% O specimen observed by microtomography

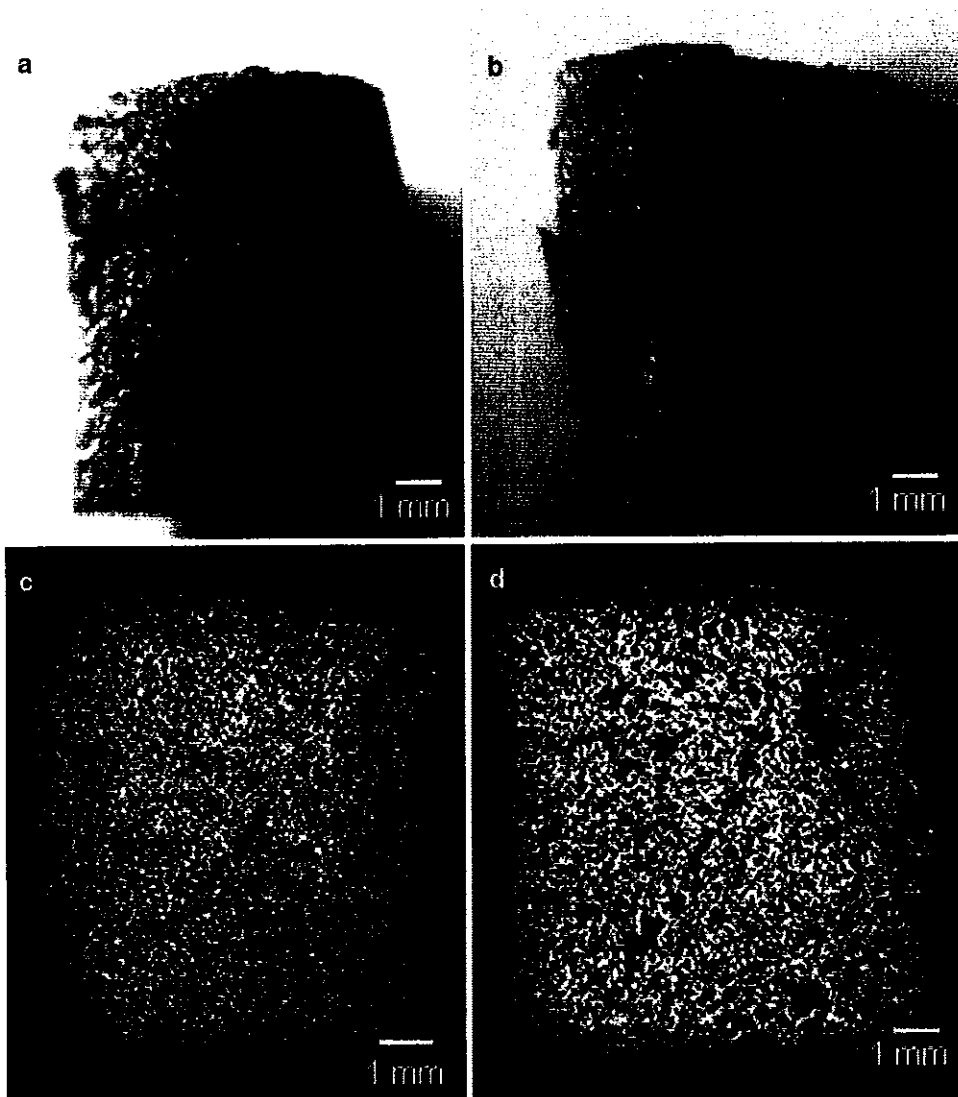
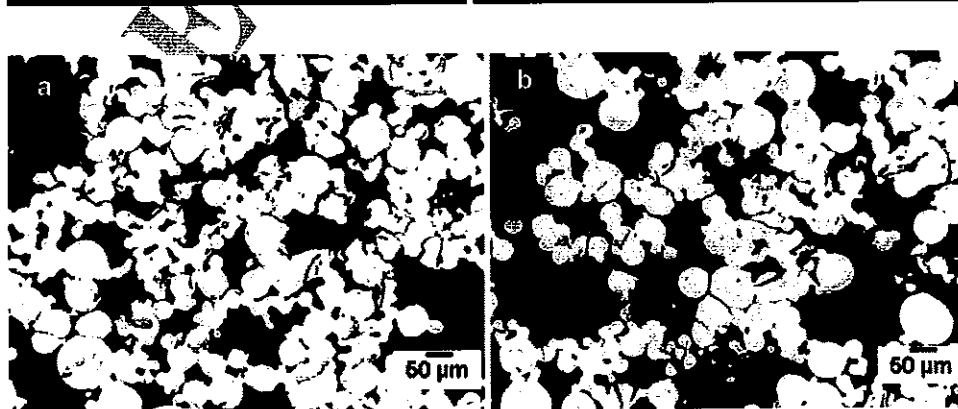


Fig. 11 Polished cross sections of the specimens at the end of the fatigue tests at 107 MPa (22.5% total deformation): **a** 0.24 wt% O specimen and **b** 0.51 wt% O specimen (arrows are pointing at microcracks)



326 specimens, containing 0.24, 0.42 and 0.51 wt% O, is
 327 observed in Fig. 12a. When all the specimens are consid-
 328 ered, the fatigue limit all fitted in the 92 MPa ± 12 MPa
 329 range. The normalized S-N curves presented in Fig. 12b
 330 suggest a difference in fatigue behavior between the lowest
 331 and highest oxygen contents (0.24 vs. 0.51 wt% O). It

should be noted that the specimens containing 0.42 and
 0.51 wt% O did not show a different behavior in fatigue,
 probably as a result of their yield strengths that did not
 differ significantly (approximately 10%).

The fracture surface observed on specimens containing
 0.24 and 0.51 wt% O (Fig. 14) shows that in both cases,

332
 333
 334
 335
 336
 337

Author Proof

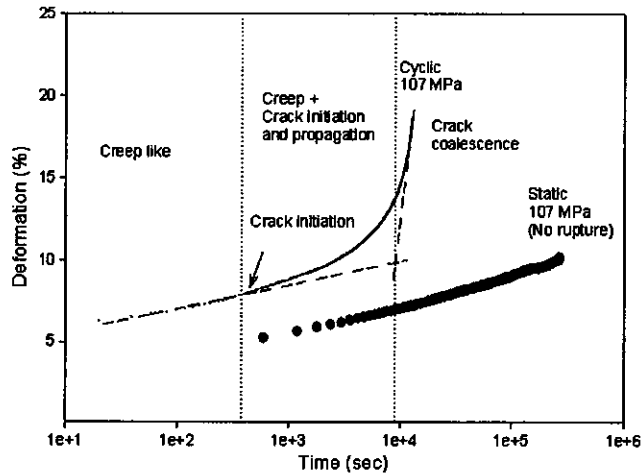


Fig. 12 Cumulative deformation versus time curves for specimens containing 0.24 wt% O in solution under two different charging modes: static (i.e. creep) and dynamic (10 Hz, $R = 0.1$)

338 quasi-cleavage is observed. However, ductile dimples were
 339 also observed on the fracture surface of the specimens with
 340 the lower oxygen content (i.e. 0.24 wt% O). This is consis-
 341 tent with observations done under monotonic compression
 342 testing [21].

343 4 Discussion

344 The amount of oxygen in solution has a clear effect on the
 345 compression behavior of the titanium foams under mono-
 346 tonic loading. While the smooth compression curves sug-
 347 gest that both materials are ductile, the specimens with
 348 smaller oxygen content (i.e. 0.24 wt% O) were signifi-
 349 cantly more ductile, which limited considerably the for-
 350 mation of cracks during monotonic deformation. The
 351 titanium foams containing larger amount of oxygen are
 352 more brittle, which leads to the formation of cracks that

propagate during deformation. The formation of cracks and
 the damage of the specimens during monotonic compression
 postpone the densification stage and cause the slope of
 the densification stage to be smaller (Fig. 4). Indeed,
 the effective cross section of the specimen contributing to
 the densification at the end of the tests was smaller in the
 brittle specimens.

The increase of the yield strength with the oxygen content
 is consistent with observations done on dense titanium
 where the yield strength ($\sigma_{0.2}$) in tension typically
 increases from 170 to 480 MPa when the oxygen content
 increases from 0.18 to 0.4 wt%. Direct comparison cannot,
 however, be done since the deformation mechanisms of
 porous materials in compression are very different from
 those observed during the deformation of dense materials
 in tension.

The cumulative cyclic deformation curves are composed
 of three stages. The first stage corresponds to a linear
 regime, where the average deformation is increasing at a
 constant rate and the deformation amplitude is relatively
 constant (Figs. 8, 9). The deformation rate during this
 stage is similar to the one observed during the creep test
 (Fig. 12). This suggests that “creep like” deformation or
 ratcheting occurs during the initial portion of the com-
 pression-compression fatigue tests. This behavior has been
 reported for other types of metallic foams [22]. The
 second stage of the cyclic loading curve is observed when
 the cumulative deformation rate increases and the curve
 deviates from linearity. During this stage, cracks are ini-
 tiated at different locations in the specimens but do not
 propagate rapidly as a result of the heterogeneous structure
 of the foams. In the present case, cracks in cell walls are
 stopped by pores or windows in the structure. The rupture
 of the cell walls forces the redistribution of the internal
 load, which leads to the formation of new cracks. Even-
 tually, the increased concentration of microcracks leads to
 crack coalescence and the rapid collapse of the specimens.

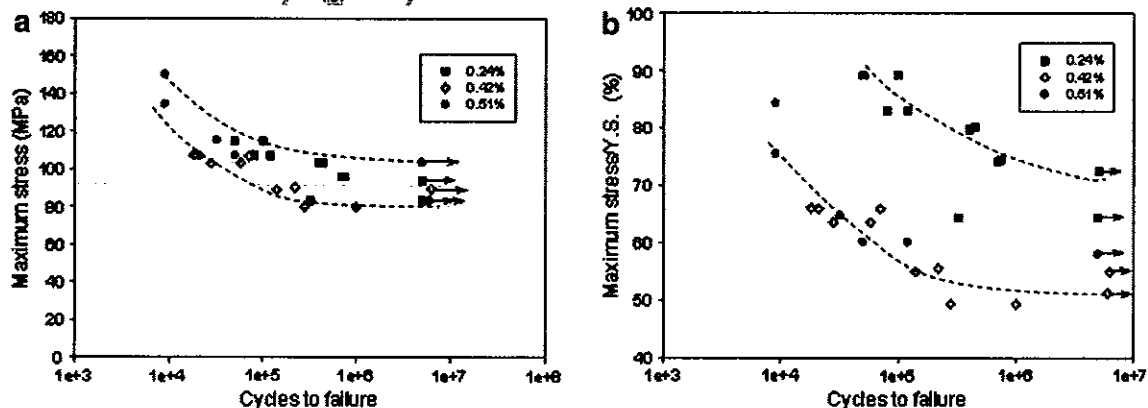
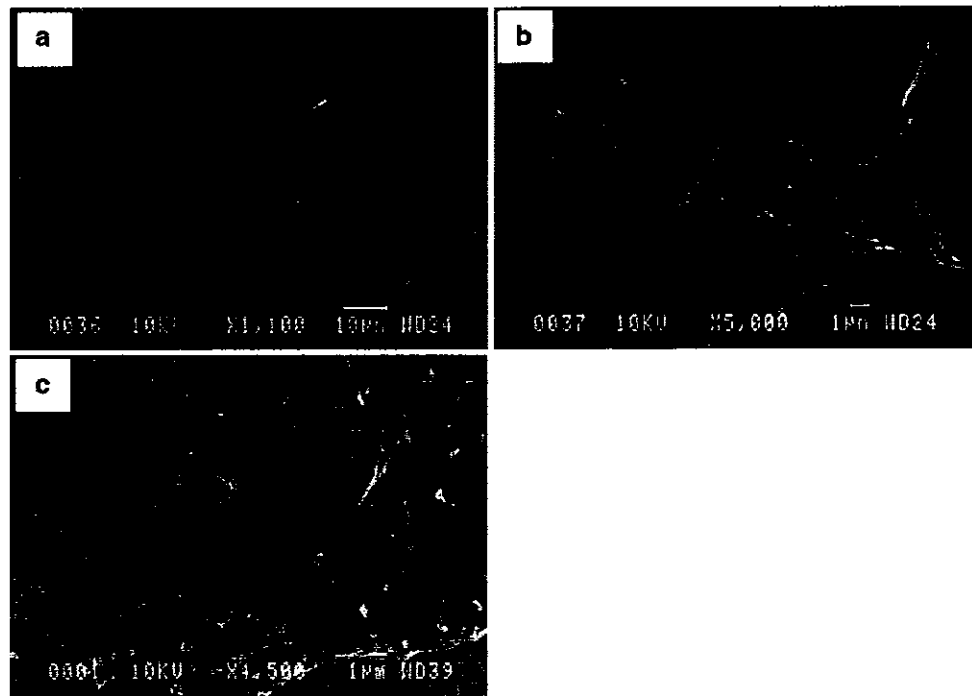


Fig. 13 Fatigue data for titanium foams with 0.24, 0.42 and 0.51 wt% oxygen in solution: **a** maximum stress and **b** maximum stress relative to the yield strength

Fig. 14 Fracture surfaces after cycling **a** 0.24 wt% O in solution, **b** 0.24 wt% O in solution at higher magnification, **c** 0.51 wt% O in solution



390 This corresponds to the onset of the third stage observed in
391 Fig. 8. While all specimens have cracks distributed in their
392 structure after 22.5% of cyclic deformation, the presence of
393 large cracks and the formation of debris during the tests
394 were more important in the specimens containing higher
395 oxygen content, due to their more brittle nature. Difference
396 in ductility were in fact observed on the fracture surface of
397 the specimens (Fig. 14). It was, however, difficult to
398 extract much information from the fracture surfaces since
399 the loading and deformation patterns in these porous
400 materials are very complex and fracture surfaces are partially
401 damaged during the tests.

402 The slope of the third stage is steeper in the foams with
403 higher oxygen content, indicating a faster collapse in these
404 specimens. While microcracks were observed in the spec-
405 imens that failed during the cyclic tests at 107 MPa, mi-
406 crocracks were not observed in the specimens exposed to a
407 107 MPa static load for the same period of time. Accord-
408 ingly, their formation is directly associated with the cyclic
409 deformation mode observed during the fatigue tests.

410 It is recognized that porous metals and metallic foams
411 behave differently than dense materials under static and
412 cyclic loading. In foams, cyclic creep or ratcheting can be
413 observed under non-zero mean stresses [22]. In compres-
414 sion-compression fatigue (load ratio >1), large cumulative
415 plastic strains gradually develop and the material behaves
416 in a quasi-ductile manner. The underlying mechanism is a
417 combination of distributed cracking of the cell walls and
418 edges and cyclic ratcheting under non-zero mean-stress
419 leading to a progressive crushing of the cells [22].

The effect of the amount of oxygen in solution on the
S-N curves (10 Hz, $R = 0.1$) is not important for the
materials and oxygen range investigated in this study (i.e.
0.24–0.51 wt% O), despite the fact that the foams with
higher content of oxygen are more brittle. However, when
the maximum stress is divided by the yield strength of the
foam, an effect of oxygen in solution can be observed. The
relative fatigue limit of the 0.24 wt% O foams is approx-
imately 70% of its yield strength while that of the
0.51 wt% O foam is approximately 52% of its yield
strength. These observations suggest that the fatigue limit
is not only affected by the yield strength but also by the
ductility. This finding differs from observations reported in
the literature on dense titanium in tension, where fatigue
limit are generally 65–70% of the yield strength of the
materials. For example, Lutjering and Williams [23]
showed that the high cycle fatigue in tension ($R = -1$) at
 10^7 cycles of grade 3 (0.35 wt% O) and grade 4 (0.4 wt%
O) titanium increases with the oxygen content and that the
fatigue strength is approximately 70% of the yield strength
of the material. Wagner and Bigoney [24] observed that the
high cycle fatigue resistance of titanium increases from 145
to 320 MPa when the oxygen content ranged from 0.13 to
0.46 wt%. Conrad [3] compiled the results from various
investigators on the fatigue limit of dense titanium with
oxygen content varying between 0.1 and 0.37 wt% O and
showed that the fatigue limit is generally around 65% that
of the yield strength.

This difference between the fatigue behavior in tension
of dense titanium and that of titanium foams under

450 compression may be attributed to the different deformation
451 modes observed. During cyclic loading of metallic foams
452 under compression, the stresses are not uniformly distrib-
453 uted in the specimens and lead to simultaneous compres-
454 sion, tension and shear loading. Fatigue cracks are formed
455 in various areas of the foam depending of the local load
456 path. The failure of a cell wall forces the load path to be
457 transferred to other portions of the specimen. Due to this
458 mechanism, the specimen can support a significant number
459 of cycles before failure occurs. However, when a suffi-
460 ciently high density of microcracks is reached, crack coa-
461 lesence is observed, which leads to the formation of larger
462 cracks, generally at 45° with respect to the loading direc-
463 tion. Portions of the structure can then detach and be
464 ejected, which leads to a reduction of the specimen cross
465 section. This second failure mechanism could explain the
466 influence of ductility on the fatigue behavior of titanium
467 foam and, therefore, the effect of oxygen on the relative
468 fatigue limit.

469 The fatigue limit at 5×10^6 cycles of the specimens
470 characterized in this study fits in the 92 MPa \pm 12 MPa
471 range. These values are significantly larger than those
472 observed with other metallic foams (Ta and Ni-Ti) inten-
473 ded for orthopedic applications [16–19]. This may be
474 partially attributed to the higher relative density of the
475 specimens characterized in this study. The values obtained
476 are also significantly larger than the fatigue limit observed
477 for dense cortical bone [25–27] and should be sufficient for
478 the design of various structural and load bearing biomed-
479 ical devices. Besides, the fatigue limit cannot be simply
480 predicted from the yield strength of the material since the
481 fatigue limit is not only linked to the yield strength of the
482 material.

483 5 Conclusions

484 Titanium foams with different oxygen contents were char-
485 acterized to evaluate the effect of oxygen on their compres-
486 sion behavior under static and cyclic loading. While the
487 results obtained showed that oxygen in solution has a sig-
488 nificant impact on the yield strength and the ductility of the
489 foams, the effect of oxygen on the S-N curves (10 Hz,
490 $R = 0.1$) is not important for the materials and oxygen range
491 investigated in this study (i.e. 0.24–0.51 wt% O). This is
492 attributed to the combined effect of the increased yield
493 strength and the reduction of the ductility when the oxygen
494 content increases. This finding differs from observations
495 reported in the literature on dense titanium in tension, where
496 fatigue limits are approximately 65–70% of the yield
497 strength of the materials. During cyclic loading, the defor-
498 mation of the foams is a combination of creep-like defor-
499 mation and fatigue. During the initial stage of deformation,

500 creep-like or ratcheting is the predominant deformation
501 mechanism up to the appearance of microcracks distributed
502 uniformly in the specimens. The coalescence of the cracks
503 appears to be the governing mechanism for the final failure
504 of the specimens. The fatigue limit at 5×10^6 cycles in the
505 range 92 MPa \pm 12 MPa were obtained for all specimens
506 characterized in this study. This is significantly larger than
507 the fatigue limit generally observed on other metallic foams
508 intended for orthopedic applications as well as on dense
509 cortical bone.

Acknowledgments The authors would like to acknowledge
510 J.-P. Nadeau, S. Mercier, M. Plourde, D. Simard, F. Borgis and
511 Dr. S. Lang for their contributions in the experimental work.
512

References 513

- 514 1. Cameron HU, Pilliar RM, McNab I. The effect of movement on
515 the bonding of porous metal to bone. *J Biomed Mater Res.*
516 1973;7(4):301–11.
- 517 2. Bobyn JD, Pilliar RM, Cameron HU. The optimum pore size for
518 the fixation of porous surfaced metal implants by the ingrowth of
519 bone. *Clin Orthop Relat Res.* 1980;150:263–70.
- 520 3. Conrad H. Effect of interstitial solutes on the strength and ducti-
521 lity of titanium. *Prog Mater Sci.* 1981;26:123–403.
- 522 4. Murray JE, Wriedt HA. The O-Ti (oxygen-titanium) system.
523 *Bull Alloy Phase Diagrams.* 1987;8:148–65.
- 524 5. Ottaviani G, Nava F, Quierolo G, Iannuzzi G, De Santi G, Tu KN.
525 Low temperature oxygen dissolution in titanium. *Thin Solid*
526 *Films.* 1987;146:201–7.
- 527 6. Wasz ML, Brotzen FR, McLellan RB, Griffin AJ Jr. Effect of
528 oxygen and hydrogen on mechanical properties of commercially
529 purity titanium. *Int Mater Rev.* 1996;41(1):1–12.
- 530 7. ASTM standard F 67-00, Standard Specification for Unalloyed
531 Titanium, for Surgical Implant Applications (UNS R50250, UNS
532 R50400, UNS R50550, UNS R50700).
- 533 8. ASTM standard F 1341-99, Standard Specification for Unalloyed
534 Titanium Wire UNS R50250, UNS R50400, UNS R50550, UNS
535 R50700).
- 536 9. ASTM standard F 1108-97a, Standard Specification for Titanium
537 and Titanium-6 Aluminum-4 Vanadium Alloy Casting for Sur-
538 gical Implants (UNS R56406).
- 539 10. ASTM standard F 136-98, Standard Specification for Wrought
540 Titanium-6 Aluminum-4 Vanadium ELI (Extra Low Interstitial)
541 Alloy (UNS R56401) for Surgical Implant Applications.
- 542 11. ASTM standard F 1472-02a, Standard Specification for Wrought
543 Titanium-6 Aluminum-4 Vanadium Alloy for Surgical Implant
544 Applications (UNS R56400).
- 545 12. ASTM standard F 1580-01, Standard Specification for Titanium
546 and Titanium-6 Aluminum-4 Vanadium Alloy Powders for Coat-
547 ings of Surgical Implants.
- 548 13. Yue S, Pilliar RM, Weatherly GC. The fatigue strength of porous-
549 coated Ti-6Al-4V implant alloy. *J Biomed Mater Res.* 1984;18:
550 1043–58.
- 551 14. Cook SD, Georgette FS, Skinner HB, Haddad RJ Jr. Fatigue
552 properties of carbon- and porous-coated Ti-6Al-4V alloy.
553 *J Biomed Mater Res.* 1984;18(5):497–512.
- 554 15. Fragomeni JM. *J Adv Mater.* 2001;33:3.
- 555 16. Arciniegas M, Aparicio C, Manero JM, Gil FJ. *J Eur Ceram Soc.*
556 2007;27.

557	17. Sevilla P, Aparicio C, Planell JA, Gil FJ. <i>J Alloy Comp.</i> 2007;439:67.	572
558		573
559	18. Barrabés M, Sevilla P, Planell JA, Gil FJ. <i>Mater Sci Eng C.</i> 2008;28:23.	574
560		575
561	19. Zardiackas LD, Parsell DE, Dillon LD, Mitchell DW, Nunnery LA. Structure, metallurgy, and mechanical properties of a porous tantalum foam. <i>J Biomed Mater Res.</i> 2001; 58(2):180–7.	576
562		577
563	20. Lefebvre LP, Thomas Y. Method of Making Open Cell Material, US patent 6,660,224 B2, Dec. 9, 2003.	578
564		579
565	21. Lefebvre LP, Baril E. Effect of oxygen concentration and distribution of the compression properties of titanium foams. <i>Adv Eng Mat.</i> 2008;10(9):868–76.	580
566		581
567	22. Ashby MF, Evans A, Fleck NA, Gibson LJ, Hutchinson JW, Wadley HNG. <i>Metal Foams. A design Guide.</i> Cambridge: Butterworth Heinemann; 2000.	582
568		583
569	23. Lütjering G, Williams JC. <i>Titanium.</i> 2nd ed. Springer: Pirna; 2007. p. 188.	584
570		585
571	24. Ashby MF, Evans A, Fleck NA, Gibson LJ, Hutchinson JW, Wadley HNG. <i>Metal foams. A design guide.</i> Cambridge: Butterworth Heinemann; 2000.	
	25. Zioupos P, Gresle M, Winwood K. Fatigue strength of human cortical bone: age, physical, and material heterogeneity effects. <i>J Biomed Mat Res A.</i> 2008;86A(3):627–36.	
	26. Choi K, Goldstein SA. A comparison of the fatigue behaviour of human trabecular and cortical bone tissue. <i>J Biomech.</i> 1992;25:1371–81.	
	27. Carter DR, Hayes WC. Compact bone fatigue damage. I. Residual strength and stiffness. <i>J Biomech.</i> 1977;10:325–37.	

UNCORRECTED PROOF

Author Proof